Topological-charge-driven reversal of ferromagnetic rings via 360° domain-wall formation

A. L. Gonzalez Oyarce,[1,*] T. Trypiniotis,[1,2] P. E. Roy,[1] and C. H. W. Barnes[1]
[1]*Cavendish Laboratory, Physics Department, University of Cambridge, Cambridge CB3 0HE, United Kingdom*
[2]*Department of Physics, University of Cyprus, 1678 Nicosia, Cyprus*
(Received 21 September 2012; revised manuscript received 24 February 2013; published 6 May 2013)

We study the reversal mechanism between opposite closed flux states of ferromagnetic nanorings driven by an azimuthal magnetic field. The reversal proceeds via the formation of 360° domain walls, and we show that the role of interacting nucleation sites is essential for the process to take place. Such nucleation is seen to create domain walls with the right topological charge conditions for 360° domain-wall formation. Given the symmetry of the system, we utilize an energetic description as a function of the azimuthal field magnitude, which clearly reveals the different stages of this reversal process. The annihilation of the 360° domain walls that is necessary for the reversal process to complete is controlling the field value at the final stage of the process. Such a fundamental mechanism for ring reversal has several implications and will guide the design of the various data-storage-device proposals based on nanorings.

DOI: 10.1103/PhysRevB.87.174408 PACS number(s): 75.60.Jk, 75.60.Ch, 75.70.−i

I. INTRODUCTION

Recent advances in the understanding of the physics of nanometer-scale devices have opened the door for ferromagnetic nanorings to be proposed as magnetic random access memory,[1,2] spin-wave generators,[3] magnetic memory recording devices,[4–6] and magnetic sensors.[7–9] Previous research on the reversal mechanisms of ferromagnetic nanorings[10–13] shows that, when an external homogeneous in-plane magnetic field is applied, two states are commonly found, the so-called "onion"and "vortex" states, the first one with two 180° domain walls (DWs) at opposite ends of a nanoring and the second with a closed flux (CF) state on which the magnetization is curled clockwise or anticlockwise.[1,10,14,15]

In general terms, the behavior of the transverse domain walls (TDWs) has been characterized in a wide range of systems and under several different types of interactions: in thin films, in nanowires, and more recently, their response to spin transfer torque.[6,16–21] Despite the interest of the scientific community in TDWs and considering that 360° DWs are often the result of the combination of two of these magnetic textures, 360° DWs have not been extensively studied. A 360° DW is the magnetic texture which allows a magnetization to rotate 360° along its length [see Figs. 1(a) and 1(b)]. Furthermore, 360° DWs have been reported in the reversal process of thin films as the results of pinning defects,[22–24] and recently, they have also been observed during the reversal process of closed structures even without the presence of any apparent pinning defects.[1,25] Recently, Goldman *et al.*[26] described the energetic properties of the annihilation process of 360° DWs by azimuthal fields generated by an electric current in permalloy (Py) nanorings.

In terms of the topological description of magnetic textures, the theory developed by Tchernyshyov and Chern[27] considers that vortices and antivortices are topological defects with topological charges of ± 1; this is also known as the winding number. On the other hand, edge charges are considered to have half-integer topological charges with values of $\pm 1/2$. By describing 360° DWs in terms of topological charges, we can see that they are formed by four edge charges with values of $\pm 1/2$,[27,28] hence, they could be understood as the combination of two TDWs with two edge charges or an even number on each side of the stripe in contrast with the single defect or odd number in the case that a single TDW is present [Figs. 1(a) and 1(b)]. The effects of such magnetic textures and their topological charges have been observed by Kunz,[28] Kunz and Priem,[29] and Kunz and Rentsch[30] while performing micromagnetic simulations of domain-wall collisions; further experimental evidence has been given by Castaño *et al.*[31] and Jang *et al.*[32] on closed thin-film geometries, characterizing the reversal process of nanorings driven by homogeneous in-plane fields. Furthermore, the existence of 360° DWs in the switching process of ferromagnetic nanorings was predicted if TDWs with the right topological charge are nucleated.[27,28,33]

In this paper, we report a similar behavior, under applied azimuthal fields having a decay of $1/r$. This $1/r$ decay was used in order to emulate the effect of a current-carrying wire that goes through the axis of the ring, considering that $\mathbf{B} = \mu_0 \mathbf{I}/2\pi r$. In this process, as the magnitude of this external magnetic field was increased, it led to a switching of the ring, from one CF state to one with the opposite vorticity [see Fig. 1(c)]. During such a reversal process, it was found that it was dominated by the nucleation of 360° DWs as suggested in Ref. 27. Hence, we were able to study both nucleation and annihilation of 360° DWs besides providing a deeper understanding of the interplay of the energies involved in addition to the topological description of these magnetic textures. Finally, we show that the presence of interacting nucleation sites is critical in the nucleation of the constituent TDWs with the right topology that will result in 360° DW formation upon their collision.

This paper is organized as follows: Sec. II is devoted to an explanation of the theoretical framework and the simulation details used. Section III shows the main results obtained and the energetic analysis performed, followed by a discussion. Finally, in Sec. IV, the main implications of this research are summarized.

II. METHODOLOGY AND SIMULATION DETAILS

In order to simulate the reversal process of ferromagnetic nanorings driven by an azimuthal field, we added appropriate

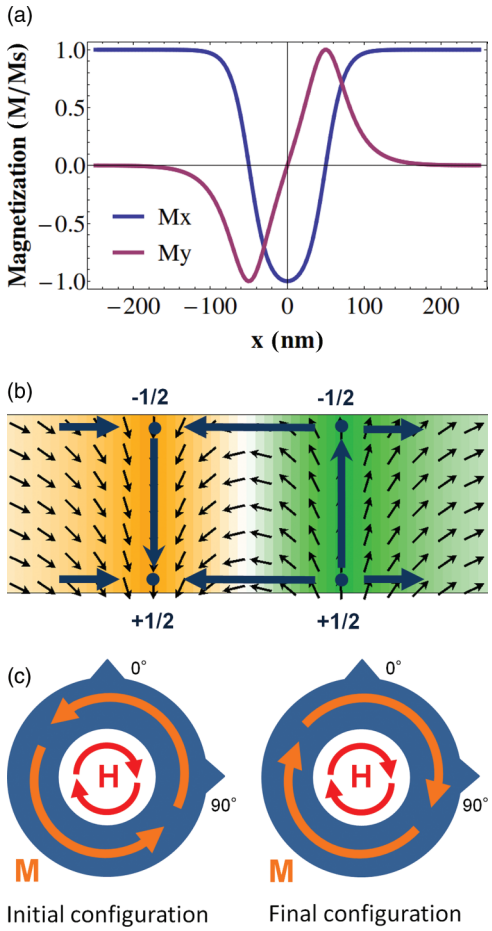

FIG. 1. (Color online) (a) Magnetization profile of a typical 360° DW. (b) Graphical representation of a 360° DW in a wire, composed out of four edge charges with values of $\pm 1/2$, respectively, as defined in Ref. 27. (c) Schematic of simulation geometry, initial and final stages.

nucleation sites in the form of triangular antinotches. This allows us to control the number of nucleation sites, their location, and the strength of the nucleation fields.[34] The antinotches are found to reduce the critical field at which the 360° DWs are nucleated compared to the case of a perfect ring. Moreover, the magnetic charge that is created by the addition of such antinotches, initializes the nucleation of TDWs with the necessary topological charge in the nucleated TDWs, hence, they can form a 360° DW.[28,29,35] The system described in Fig. 1(c) undergoes a magnetization reversal process driven by an azimuthal magnetic field with a decay of $1/r$ in which magnitude was increased in steps of 2.5 mT. The simulations were carried out for a permalloy nanoring with an outer radius of 200 nm, an inner radius of 100-nm thickness, 4 nm without magnetocrystalline anisotropy, and two antinotches at 0° and 90° as shown in Fig. 1(c). The value of exchange stiffness A used was 13 pJ/m, and the saturation magnetization M_s was 860 kA/m. The simulations were carried out using the numerical package OOMMF,[36] which is based on the finite-difference discretization method which introduces artificial nucleation points because a square discretization grid is used, hence, it produces discontinuities at the boundaries of the ring. It is expected that the effect of a coarse discretization grid is

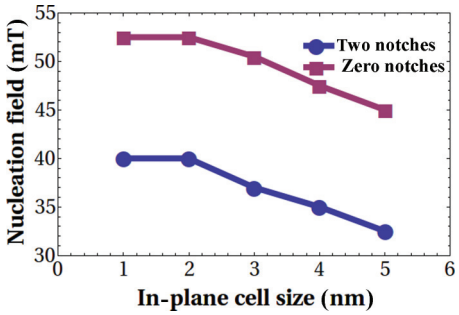

FIG. 2. (Color online) The effect of cell size on the critical field at which nucleation occurs for rings of outer radius 200 nm and inner radius 100 nm.

attenuated at sufficiently small cell sizes. In order to quantify the effect of the discretization grid in the simulations, the dependency of the nucleation field for 360° DWs was studied as shown in Fig. 2.

The results of Fig. 2 show the effect of the in-plane cell size on the value of the nucleation field. For a cell size smaller than 2×2 nm^2, the value of the nucleation field remains constant and unaffected by the size of the cell size used. The use of a 2×2-nm^2 cell size represents an optimal compromise between accuracy and speed of the simulations. In the case of no antinotches, there is still nucleation due to nucleation sites produced by the discretizing grid. In this case, the nucleation field is higher as the coarse discretizing grid produces less artificial magnetic charge in comparison with the ring that has antinotches.

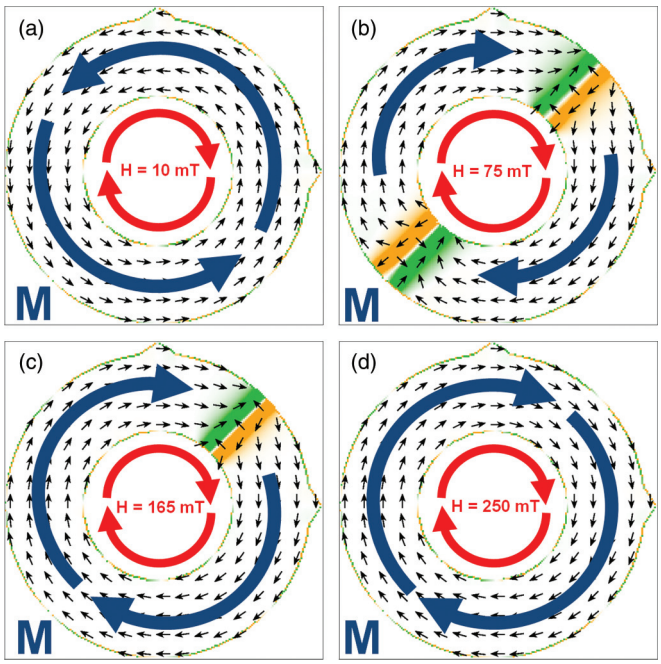

FIG. 3. (Color online) Characteristic stages of the reversal process for an antinotched ring with a 200-nm outer radius, a 100-nm inner radius, and a 4-nm thickness. The divergence of the magnetization is shown in green and orange. The thick arrows serve as guides to the eye.

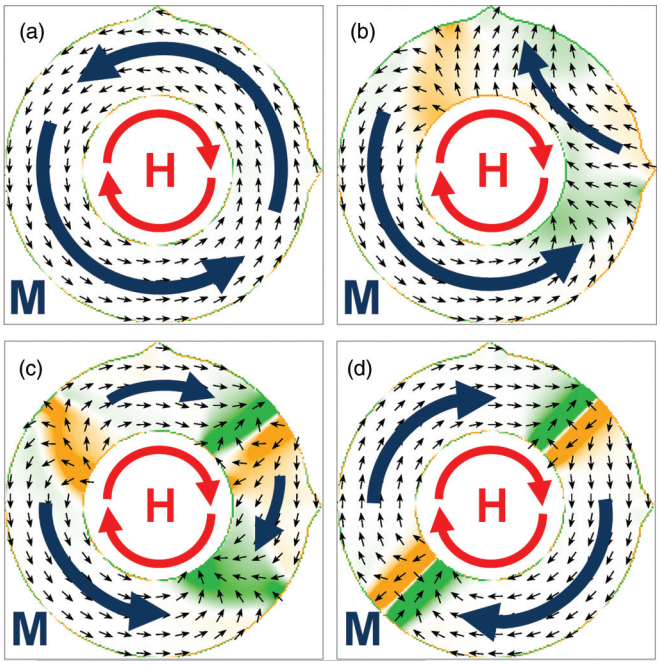

FIG. 4. (Color online) Snapshots of the magnetization during the nucleation process of 360° DWs after the nucleation field is reached. (a) and (b) show the winding of the magnetization in the sectors surrounding the antinotches, whereas, (c) and (d) show the stabilization process during which 360° DWs are formed. The total time of this process is ∼150 ps. The divergence of the magnetization is shown in green and orange. The thick arrows serve as guides to the eye.

In order to reverse the magnetization of the ring, we considered the ring in the initial state as shown in Fig. 1(c) (left), and then, we applied an azimuthal field of opposite vorticity to the magnetization. The magnitude of the azimuthal field was increased in small steps of 2.5 mT, and the magnetization was relaxed at each value of the field. As the magnitude of the external magnetic field was increased, 360° DWs were nucleated at a certain field value and remained stable until the full reversal of the magnetic ring took place at a higher field value. The final configuration of the ring is a CF state with opposite vorticity than the initial state as shown in Fig. 1(c) (right).

III. RESULTS AND DISCUSSION

Following the methodology explained in Sec. II, the reversal behavior of a Py nanoring with an outer radius of 200 nm, an inner radius of 100 nm, and a thickness of 4 nm is studied. The main stages of the switching process are shown in Fig. 3 where it can be seen that such a process is dominated by the nucleation and annihilation of 360° DWs while conserving topological charge, see Fig. 7. Initially, the ring is in an anticlockwise CF state as shown in Fig. 3(a) until the nucleation field is reached and two 360° DWs are formed, Fig. 3(b). It is worthwhile noting that the nucleation field is much higher than the depinning field associated with the antinotch[37] due to the high field at which the walls are nucleated.[38] Moreover, the value of the nucleation field is dependent on the height of the antinotch, which, in this case, is chosen to be about 1/6th of the ring width. If the height of the antinotch is increased, the value of both fields could change by up to 70% as observed in other studies.[29,38] The value of the nucleation field could play a very important role in device design as previously suggested.[39,40] Unlike previous papers where the emphasis has been on the pinning effects of the notches and antinotches,[29,35] our results show how antinotches can act as controllable nucleation sites for TDWs with the right topological charge in order to form 360° DWs. Even though the pinning potential of such antinotches is present during the motion of TDWs and depends on the topological charges involved,[29] the magnitude of this interaction is not strong enough to stop or cancel the formation of 360° DWs. Here, we have selected the size of the antinotches so that the nucleation field is lower than that due to the discretization in the case where no antinotches exist, whereby, the rough grid creates nucleation points. Furthermore, we made sure that the pinning field for the TDWs is lower than the nucleation field. It is worth noting that the same behavior is observed if the antinotches are placed at 0° and 90°, as shown in Fig. 1, 45° and 135° or if they are rotated by any other angle.

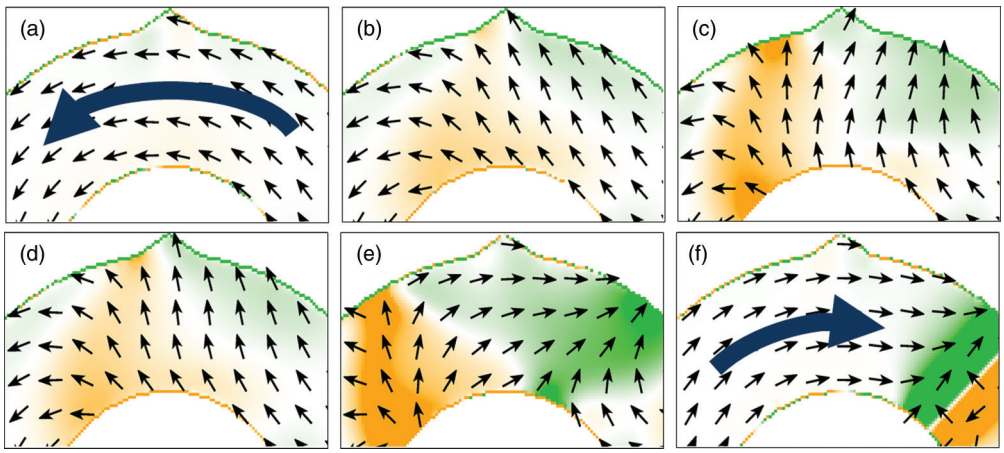

FIG. 5. (Color online) Snapshots of the nucleation process in the vicinity of the upper antinotch, which involves the formation of a reverse domain. Furthermore, when the other antinotch is added to the picture, the process conserves the topological charge as defined by Ref. 27 and shown in Fig. 7. The divergence of the magnetization is shown in green and orange. The thick arrows serve as guides to the eye.

After the two walls are formed, they stabilize at opposite sections of the ring, Fig. 3(b). When the first annihilation field is reached, the left DW is destroyed, Fig. 3(c). According to Ref. 26, this process occurs because this wall has the same circulation as the vortex state of the ring, hence, providing a smaller energy barrier for the field to reverse it. Finally, in Fig. 3(d), the system continues the reversal process until it completely reverses its magnetization to a stable clockwise CF state by a subsequent destruction of the second 360° DW.

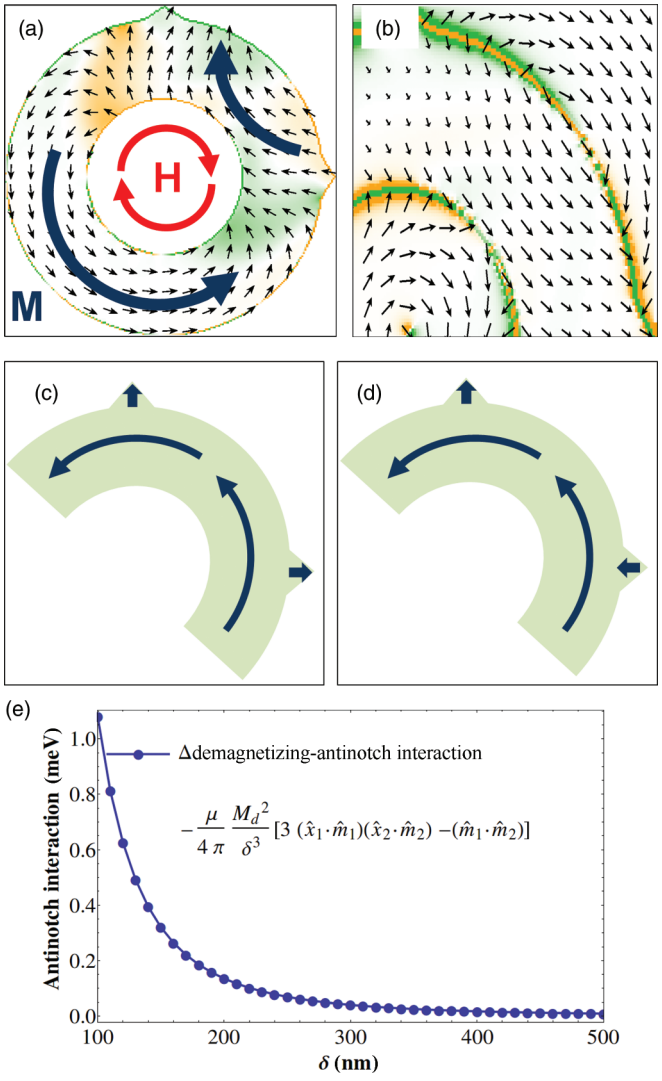

FIG. 6. (Color online) (a) and (b) Magnetization and total field during the nucleation phase of the TDWs that will form the 360° DW. The thick arrows serve as guides to the eye. The divergence of the magnetization and total field is shown in green and orange. (c) and (d) The two different configuration possibilities that could arise at the antinotches during the formation of reverse domains. The total field of (b) is similar to the one that arises from the configuration in (d), the schematic for the possible magnetization configurations at the antinotches just before nucleation. (e) Energetic barrier of the dipole-dipole approximation for the magnetostatic interaction between the two possible magnetic configurations of the antinotches at different distances. For the distance at which the antinotches are located 382.12 nm, the energy barrier is about 0.019 meV, which corresponds to a temperature of 0.22 K.

The nucleation of 360° DWs across the ring proceeds as depicted by the sequence of snapshots shown in Fig. 4. After reaching the nucleation field, the area around an antinotch initiates the nucleation of a reverse domain with two TDWs on either end as seen in Figs. 4 and 5. Thus, for two antinotches, the rotation of the magnetization induces the nucleation of four TDWs. As the reverse domains expand, the TDWs from different antinotches move toward each other and collide in the middle point between the antinotches (a closer look around the upper antinotch is shown in Fig. 5). This process conserves the topological charge of the system since each of the TDWs has two edge charges of value $\pm 1/2$ (Refs. 1,27 and 28) (see Fig. 7 for more information). In Fig. 5, a closeup to the area which initiates the nucleation of the TDWs is shown, and it can be seen how the reverse domain evolves as a sector below the antinotch.

We estimate the magnetostatic interaction between the two antinotches, which initiate the nucleation of the reverse domains [see Figs. 6(a) and 6(b)]. We postulate that, if the demagnetizing energy between the antinotches is bigger than the thermal energy at room temperature, the nucleation of 360° DWs through the use of antinotches could be of statistical significance. To estimate such an interaction, we consider the two possible configurations that the system could have at the moment of nucleation as shown in Figs. 6(c) and 6(d). Furthermore, the value for M_d, see Fig. 6(e), which is the effective magnetic moment of a thin film as previously defined in Refs. 41 and 42, considers the area of the antinotches which have widths of 50 nm and heights of 25 nm, see Fig. 4(b). From Fig. 6(e), we can see that, at nucleation, the magnetostatic interaction generates an energy barrier with a value of 0.019 meV at a distance of 318.12 nm, corresponding to a temperature of 0.22 K. This evidence suggests that the demagnetizing interaction is not enough to overcome thermal effects as the nucleation of 360° DWs becomes a stochastic process. We must remark that careful design and construction in experimental devices are needed for this reversal mechanism to be avoided. We leave these behaviors for a further study.

A closer look at the role of the topological edge charges is shown in Fig. 7. In this context, the edge charges have a value of $\pm 1/2$ obtained from the line integral along the boundary as defined in Ref. 27. Making an analogy with the Coulomb interaction, the two edge charges found in TDWs are "attractive" but not with enough strength to break the edge confinement, hence, the edge effects hold the wall together,[27] conserving topological charge along the process.

Based on these phenomena, we can postulate that the presence of nucleation sites (in this case, the antinotches) is critical for this process to happen: It creates localized surface charge in order to initiate the reversal process, determining, by dipolar coupling, the chirality and the topological charge of the four walls nucleated in the system.[28,38,40] Furthermore, if we consider the top antinotch, the wall to its left is repulsed by it since it has a negative topological charge; a similar behavior has been observed by Masamitsu *et al.*[35] by suggesting that the antinotch acts like an energy barrier. On the other hand, the wall to the right of the antinotch is moved by the magnetic field as the pinning field is small compared to the nucleation field;[29] a similar process occurs for the antinotch situated to the right.

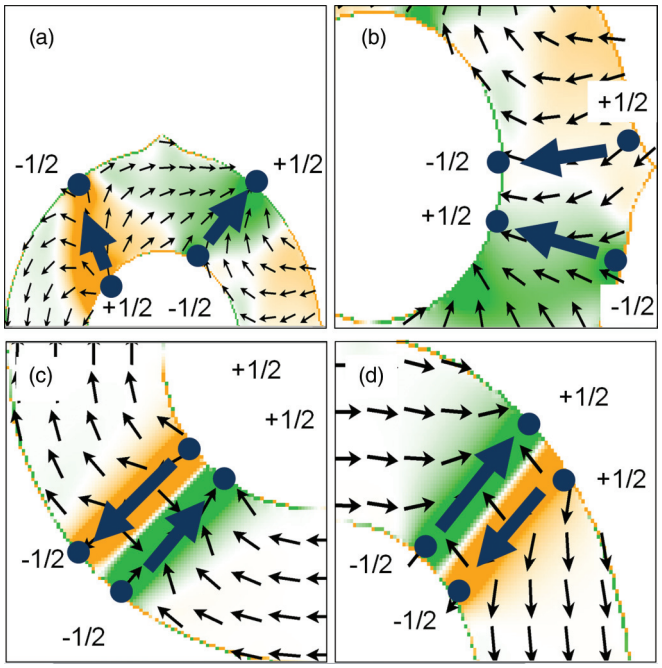

FIG. 7. (Color online) Snapshots of the nucleation and stabilization of 360° DWs at the antinotches and the localization of the half-integer topological charges. (a) and (b) show how the antinotches become sites of the nucleation of two TDWs with opposite half-integer topological charges, hence, conserving the total value of the topological charge. (c) and (d) show 360° DWs formed at opposite sides of the ring together with the positions of the half-integer topological charges proposed by Ref. 28. The divergence of the magnetization is shown in green and orange. The thick arrows serve as guides to the eye.

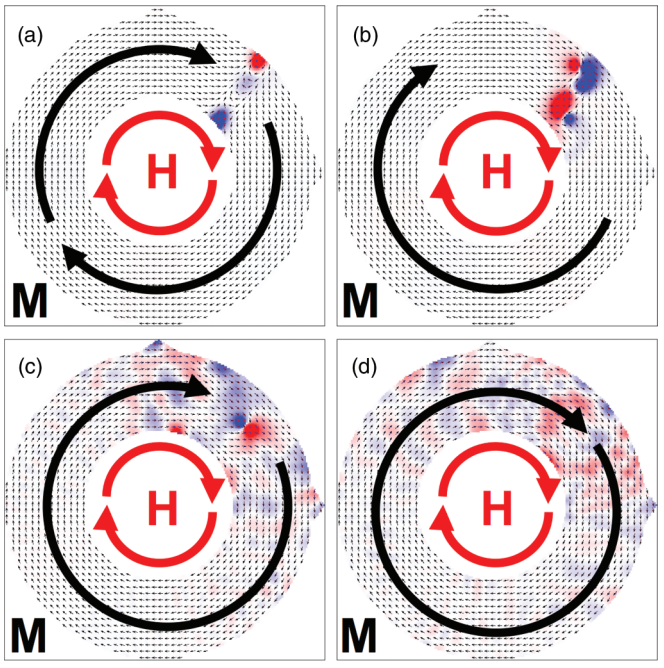

FIG. 8. (Color online) See Supplemental Material.[43] Snapshots of the annihilation process of 360° DWs. The total time interval is 27 ps. (a) Opposite sections of the ring have structures with both Z directions. (b) These two complex structures meet at the middle section of the ring in order to form only one structure with both Z directions as shown in (c). (d) Finally, the ring reverses, producing a burst of spin waves in the process. This process is akin to the one described by Mascaro and Ross[44] where the annihilation is mediated through vortices. In blue, the magnetization pointing to $+Z$ and in red, the magnetization pointing to $-Z$. The thick arrows serve as guides to the eye.

Finally, when a higher value of the applied magnetic field is reached, the annihilation of the second 360° DW takes place, and the reversal process of the ring is completed as depicted in Fig. 8. See Supplemental Material.[43] Such an annihilation process is extremely fast, taking about 50 ps to complete and results in the production of spin waves. Furthermore, the process shares some similarities with the descriptions of Mascaro and Ross[44] and Tchernyshyov and Chern[27] where it is suggested that the annihilation of 360° DWs can be used as a spin-wave generator.

A. Energetic description

Given the symmetry of the ring, the use of magnetization against field $M(H)$ plots as in conventional hysteresis loops[45] would provide no further insight about the process described here since the average M would always be zero. Hence, we rely on plots of the various energies involved in the reversal process against the field $E(H)$ as shown in Fig. 9 where we use the magnitude of the azimuthal field as the appropriate field H. The ring with no antinotches, dotted line, was discretized using $4 \times 4\text{-nm}^2$ cells. The reversal process is divided in four stages, shown in Fig. 9 for the the exchange energy. The Zeeman energy and total energy are plotted. During stage (I), the nucleation of the walls takes place, and the Zeeman energy increases as the magnetization along the ring is not aligned with the external field until the nucleation field is reached and the 360° DWs are nucleated. The value of the nucleation field is lower for antinotched rings than for rings without antinotches as they possess less magnetic charge to initiate nucleation. After a sharp transition in energies, stage (II) commences with the nucleation of two 360° DWs. The exchange energy increases, and the demagnetizing energy is decreased as the DWs are compressed by the external magnetic field. At stage (III), the first annihilation field is reached, and one wall is destroyed, occurring as a second transition in energy, for then, the exchange and demagnetizing energies continue to increase as the remaining wall is compressed. In stage (IV), the reversal process finishes with the annihilation of the remaining 360° DW. The system is characterized by sharp and well-defined transitions in terms of the azimuthal field H for both nucleation and annihilation of 360° DWs.

Furthermore, in Fig. 9, the results for a ring with nucleation sites induced by a course discretizing grid are also shown in parallel to the rings with antinotches. This artificial rough ring nucleates four walls instead of the two observed for the antinotched rings, hence, the total energy is almost four times the total energy in the case of antinotched rings. Moreover, it can be observed that the nucleation field is higher for the case without antinotches; this indicates that discretization effects are negligible in the case of antinotches. A further analysis of the artificial system is performed in the Appendix.

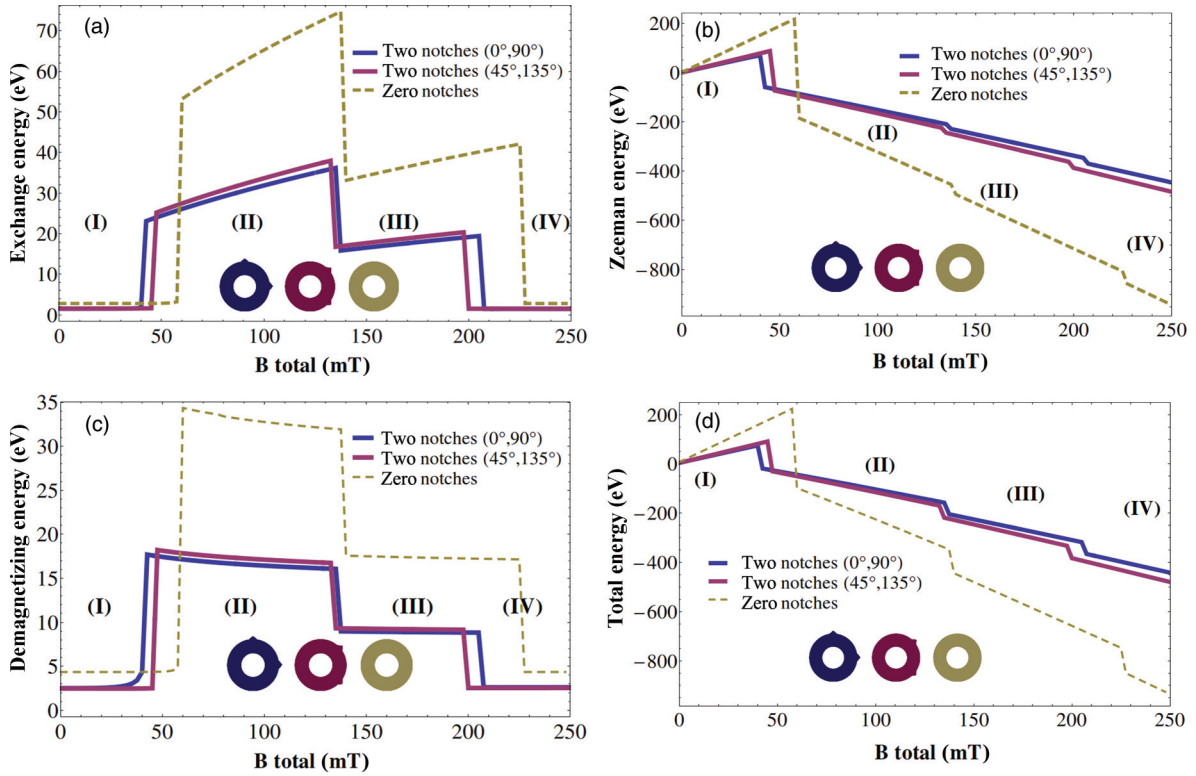

FIG. 9. (Color online) Plots of (a) exchange, (b) Zeeman, (c) demagnetizing, and (d) total energies during the reversal process where, in terms of the stages of the process, stage (I) is before the nucleation of the walls, in stage (II), 360° DWs nucleation takes place, in stage (III), the first annihilation field is reached, and one wall is destroyed, and finally, in stage (IV), the switching process finishes with the annihilation of the remaining 360° DW.

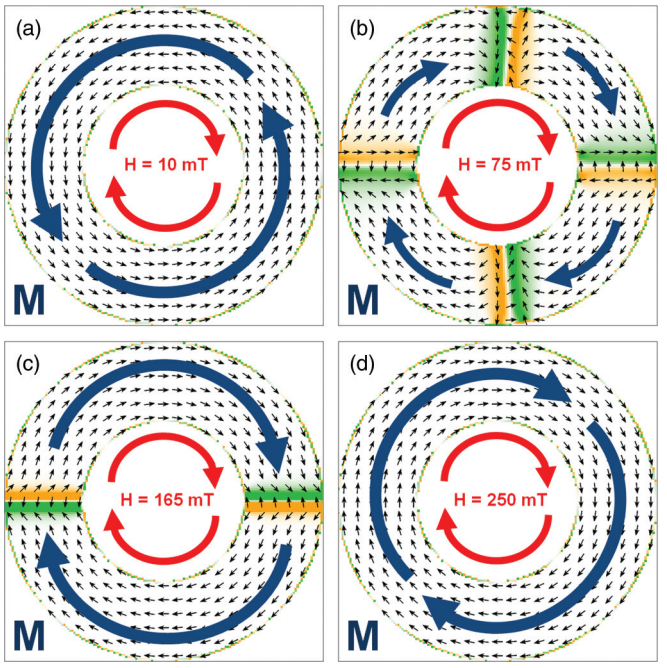

FIG. 10. (Color online) Snapshots of the main stages of the nucleation and annihilation processes of 360° DWs in a ring of outer radius 200 nm, inner radius 100 nm, and thickness 4 nm using a 5-nm^2 grid. Due the generation of artificial nucleation sites, four walls are nucleated instead of two. The divergence in the magnetization is shown in green and orange. The thick arrows serve as guides to the eye.

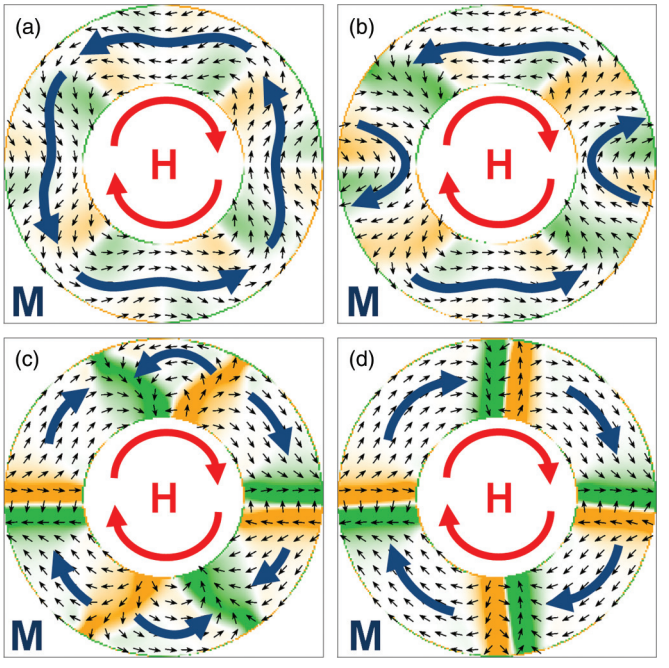

FIG. 11. (Color online) Snapshots of 360° domain-wall nucleation in a ring without antinotches. (a) and (b) describe how the process is initiated, and it localizes the nucleation points as multiples of 22.5° from the top part of the ring. (c) and (d) show that only four walls can be sustained in this geometry; in rings with outer radii bigger than 500 nm, it was found that up to eight walls could be nucleated. The divergence of the magnetization is shown in green and orange. The thick arrows serve as guides to the eye.

Regarding the final stage of the reversal process as shown in Fig. 9(d), the energy gain after the annihilation of the last wall is near 50 eV at about 200 mT, which is several times the field magnitude needed for reversal in thin films[46–48] and roughly ten times the magnitude required to reverse ring structures with uniform unidirectional in-plane fields. These relatively high annihilation fields are important factors for the design of devices involving the reversal of nanorings. If the reversal proceeds through the formation of 360° DWs, the fact that the reversal field is high can be harnessed for data stability, for example. On the other hand, if the high field is undesirable, steps should be taken to avoid 360° DW formation in the first instance.

In terms of characterization, it could be interesting to measure the magnetic properties of this wall in terms of effective parameters, such as the magnetic moment and the interaction energy between the two TDWs of which the 360° DWs are composed. Obtaining further information about these characteristics could provide insight into the energies associated with the nucleation of these magnetic textures and their possible applications to dynamical effects.[44]

IV. CONCLUSIONS

The results show that the reversal process of a nanoring driven by an azimuthal field is dominated by the nucleation of 360° DWs. It is shown that adjacent interacting nucleation sites form TDWs with the appropriate topological charge so that when they collide, they always form 360° DWs. The symmetry of the system does not allow us to gain any insight into the problem from conventional $M(H)$ hysteresis loops. Instead, we utilize an energetic description of the system as a function of the azimuthal field $E(H)$, which clearly reveals the different stages of the reversal process: beginning with a CF state, reversed via the nucleation of 360° DWs finishing with a CF state with opposite chirality to the initial one. The transitions between these stages are marked with clear sharp transitions in the different components of the total energy of the system at well specified values of the azimuthal field. The magnitude of the changes in energy during the transitions and the associated magnitude of the field make it relevant for the development of magnetic data recording devices as suggested by Refs. 1–3 and 5–9, considering that the interaction of 360° DWs with other magnetic phenomena, such as other DWs, spin currents, or even geometrical structures[4,44] could be relevant in such situations.

ACKNOWLEDGMENTS

This work was funded by the Conicyt and its program, Becas Chile. Furthermore, the calculations were carried out using the Camgrid high-throughput facility of the University of Cambridge as well using the Darwin Supercomputer of the University of Cambridge High Performance Computing Service, provided by Dell Inc. using Strategic Research Infrastructure Funding from the Higher Education Funding Council for England and funding from the Science and Technology Facilities Council.

APPENDIX

In order to get a better understanding of the reversal process in the case of no antinotches, in Fig. 10, we show the main stages of the reversal process of such a ring. It can be seen that, instead of the two 360° DWs previously observed in Fig. 3, these are now four 360° DWs. The grid generates magnetic charge to initiate the reversal mechanism. Furthermore, Fig. 11 shows the main steps after the nucleation field is reached. This process, as in the case where antinotches were present, conserves the topological charge. It is worth mentioning that, in rings with outer radii of over 500 nm, using this same technique, eight 360° DWs were observed. The corresponding $E(H)$ diagrams are equivalent to the ones shown in Fig. 9.

*alg55@cam.ac.uk

[1] F. J. Castaño, C. A. Ross, C. Frandsen, A. Eilez, D. Gil, H. I. Smith, M. Redjdal, and F. B. Humphrey, Phys. Rev. B **67**, 184425 (2003).
[2] T. J. Hayward, J. Llandro, R. B. Balsod, J. A. C. Bland, D. Morecroft, F. J. Castaño, and C. A. Ross, Phys. Rev. B **74**, 134405 (2006).
[3] P. E. Roy, T. Trypiniotis, and C. H. W. Barnes, Phys. Rev. B **82**, 134411 (2010).
[4] C. B. Muratov and V. V. Osipov, IEEE Trans. Magn. **45**, 3207 (2009).
[5] R. P. Cowburn, D. K. Koltsov, A. O. Adeyeye, M. E. Welland, and D. M. Tricker, Phys. Rev. Lett. **83**, 1042 (1999).
[6] R. Cowburn, in *International Conference on Electromagnetics in Advanced Applications, 2007. ICEAA 2007, Torino, Italy* (IEEE, Piscataway, NJ, 2007), p. 602.
[7] S. Parkin, X. Jiang, C. Kaiser, A. Panchula, K. Roche, and M. Samant, Proc. IEEE **91**, 661 (2003).
[8] J. H. Lee, S. N. Holmes, B. Hong, P. E. Roy, M. D. Mascaro, T. J. Hayward, D. Anderson, K. Cooper, G. A. C. Jones, M. E. Vickers, C. A. Ross, and C. H. W. Barnes, Appl. Phys. Lett. **95**, 172505 (2009).
[9] M. Diegel, R. Mattheis, and E. Halder, IEEE Trans. Magn. **40**, 2655 (2004).
[10] J. Rothman, M. Kläui, L. Lopez-Diaz, C. A. F. Vaz, A. Bleloch, J. A. C. Bland, Z. Cui, and R. Speaks, Phys. Rev. Lett. **86**, 1098 (2001).
[11] W. Zhang, R. Singh, N. Bray-Ali, and S. Haas, Phys. Rev. B **77**, 144428 (2008).
[12] C. A. F. Vaz and M. Klaui, J. Magn. Magn. Mater. **272-276**, 1631 (2004).
[13] L. Lopez-Diaz, M. Kläui, C. A. F. Vaz, and J. A. C. Bland, J. Phys.: Condens. Matter **15**, R985 (2003).
[14] L. D. Landau and E. M. Lifshitz, Phys. Z. Sowjetunion **8**, 135 (1935).
[15] F. J. Castaño, D. Morecroft, and C. A. Ross, Phys. Rev. B **74**, 224401 (2006).
[16] P. A. Rikvold, G. Brown, S. J. Mitchell, and M. A. Novotny, in *Nanostructured Magnetic Materials and Their Applications,*

edited by D. Shi, B. Atkas, L. Pust, and F. Mikailov, Springer Lecture Notes in Physics Vol. 593 (Springer, Berlin, 2002), p. 164.
[17]A. Mougin, M. Cormierand, P. J. Metaxas, J. P. Adam, and J. Ferre, Europhys. Lett. **78**, 57007 (2007).
[18]D. G. Porter and M. J. Donahue, J. Appl. Phys. **95**, 6729 (2004).
[19]L. O'Brien, D. Petit, E. R. Lewis, R. P. Cowburn, D. E. Read, J. Sampaio, H. T. Zeng, and A.-V. Jausovec, Phys. Rev. Lett. **106**, 087204 (2011).
[20]T. Koyama, D. Chiba, K. Ueda, K. Kondou, H. Tanigawa, S. Fukami, T. Suzuki, N. Ohshima, N. Ishiwata, Y. Nakatani, K. Kobayashi, and T. Ono, Nature Mater. **10**, 194 (2011).
[21]A. Beguivin, L. A. O'Brien, A. V. Jausovec, D. Petit, and R. P. Cowburn, Appl. Phys. Lett. **99**, 142506 (2011).
[22]P. Gaunt and C. K. Mylvaganam, J. Appl. Phys. **48**, 2587 (1977).
[23]H. S. Cho, C. Hou, M. Sun, and H. Fujiwara, J. Appl. Phys. **85**, 5160 (1999).
[24]L. J. Heyderman, H. Niedoba, H. O. Gupta, and I. B. Puchalska, J. Magn. Magn. Mater. **96**, 125 (1991).
[25]M. Redjdal, P. W. Gross, A. Kazmi, and F. B. Humphrey, J. Appl. Phys. **85**, 6193 (1999).
[26]A. Goldman, A. S. Licht, Y. Sung, and Y. Li *et al*., J. Appl. Phys. **111**, 07D113 (2012).
[27]O. Tchernyshyov and G.-W. Chern, Phys. Rev. Lett. **95**, 197204 (2005).
[28]A. Kunz, Appl. Phys. Lett. **94**, 132502 (2009).
[29]A. Kunz and J. D. Priem, IEEE Trans. Magn. **46**, 1159 (2010).
[30]A. Kunz and E. W. Rentsch, IEEE Trans. Magn. **46**, 1156 (2010).
[31]F. J. Castaño, C. A. Ross, A. Eilez, W. Jung, and C. Frandsen, Phys. Rev. B **69**, 144421 (2004).
[32]Y. Jang, S. R. Bowden, M. Mascaro, J. Unguris, and C. A. Ross, Appl. Phys. Lett. **100**, 062407 (2012).
[33]O. A. Tretiakov and O. Tchernyshyov, Phys. Rev. B **75**, 012408 (2007).
[34]C.-P. Lee, C.-J. Hsu, and M.-F. Lai, IEEE Trans. Magn. **47**, 505 (2011).
[35]M. Hayashi, L. Thomas, C. Rettner, R. Moriya, X. Jiang, and S. S. P. Parkin, Phys. Rev. Lett. **97**, 207205 (2006).
[36]M. J. Donahue and D. G. Porter, OOMMF User's Guide, Version 1.0 (NIST, Gaithersburg, MD, 1999).
[37]Extensive simulations were used to confirm that the depinning field is lower than the nucleation field.
[38]L. K. Bogart, D. S. Eastwood, and D. Atkinson, J. Appl. Phys. **104**, 033904 (2008).
[39]A. Himeno, T. Okuno, S. Kasai, and T. Ono *et al*., J. Appl. Phys. **95**, 66101 (2005).
[40]L. K. Bogart, D. Atkinson, K. O'Shea, D. McGrouther, and S. McVitie, Phys. Rev. B **79**, 054414 (2009).
[41]T. J. Hayward, M. T. Bryan, and D. A. Allwood *et al*., Appl. Phys. Lett. **96**, 052502 (2010).
[42]T. J. Hayward, M. T. Bryan, P. W. Fry, P. M. Fundi, M. R. J. Gibbs, D. A. Allwood, M.-Y. Im, and P. Fischer, Phys. Rev. B **81**, 020410 (2010).
[43]See Supplemental Material at http://link.aps.org/supplemental/10.1103/PhysRevB.87.174408 for a video of the annihilation process of 360° DWs.
[44]M. D. Mascaro and C. A. Ross, Phys. Rev. B **82**, 214411 (2010).
[45]M. Coisson, G. Barrera, F. Celegato, L. Martino, P. Tiberto, F. Vinai, and P. Allia, J. Appl. Phys. **112**, 053910 (2012).
[46]P. Haumer, H. Hauser, P. L. Fulmek, and D. Bajalan, IEEE Trans. Magn. **40**, 2745 (2004).
[47]D.-X. Chen, Y.-F. Li, L. Pascual, M. Vazquez, and A. Hernando, J. Magn. Magn. Mater. **212**, 373 (2000).
[48]Z. H. Wei, M. F. Lai, C. R. Chang, and N. A. Usov *et al*., IEEE Trans. Mag. **40**, 2107 (2004).